Packed-Bed Photocatalytic Reactors. A Packing Structure Model and Its Experimental Validation with Computerized Tomography

Horacio A. Irazoqui, Miguel A. Isla, Rodolfo J. Brandi, and Alberto E. Cassano*

Instituto de Desarrollo Tecnológico para la Industria Química (INTEC), Universidad Nacional del Litoral and CONICET, Güemes 3450, 3000 Santa Fe, Argentina

A statistical model is proposed for the description of the spatial structure of a packed bed of spherical-like particles in terms of one- and two-bead distribution functions. This is the first step toward the full modeling of the radiation field in an annular photocatalytic reactor, mainly where the interaction between radiation and the packed beads is concerned. The model has been validated against tomography experiments performed on an up-scaled packing prototype. The three-dimensional structure of its loose random packing has been digitized. On the basis of this structural information, the experimental version of the one-bead distribution function, as well as those of the conditional distribution and the solid volume fraction, could be constructed without mediating models. Then the parameters of the proposed statistical model could be determined by nonlinear regression. The agreement between the functions constructed experimentally and their model-predicted counterparts with the set of regressed model parameters is remarkable considering the highly structured shapes of their profiles. Exact relationships have been established to scale those model parameters bearing dimensions to packings with different bead radii.

Introduction

Photocatalytic reactions, catalyzed by light activated solid semiconductors, constitute one attractive possibility among Advanced Oxidation Technologies (AOT) for air and water decontamination, especially from organic compounds.[1,2] This particular technology is attractive not only because of its effectiveness in destroying contaminants but also because of its ability to be operated with solar energy. Usually, titanium dioxide is used as the catalyst.

In most cases of air or water decontamination, the modeling of a fluid−solid heterogeneous photocatalytic reactor requires (i) a fluid−solid catalyst interaction model, (ii) a radiation emission−transport−reception model, and (iii) a kinetic model for the reaction. The first aspect has been extensively treated in the chemical engineering literature, and the last one is still the subject of a wide research effort in several fields connected with environmental chemistry. This work is a contribution to the problem of the radiation field in heterogeneous reactors.

In the particular case of liquid−solid systems, most of the published work deals with small particles (30−300 nm) suspended in water. A problem only recently rigorously solved has been the modeling and experimental validation of a participating, chemically reacting medium, including light absorption and scattering in a suspended photocatalytic bed.[3] However, in the past few years, it became apparent that systems with suspended particles, although very apt for kinetic studies, have the technological drawback of the large costs associated with catalyst separation and recovery. The proposed alternative is based on the use of immobilized catalysts, including fluidized-bed reactors,[4,5] catalytic wall reactors,[6] and packed-bed reactors.[7−10]

In catalyzed wall reactors, the radiation field can be modeled without major difficulties because of the absence of light scattering.[10−13] However, in those cases where a liquid phase is being treated, the photocatalytic reaction has been found, very often, to be controlled by the limiting mass-transfer rates. Concerning photocatalytic packed-bed reactors, a first approximation has been published by Raupp et al.[7] A model for a gas−solid packed-bed reactor was described as a one-dimensional idealization based on the two-flux model for radiation transport discussed by Maruyama and Nishimoto.[14] With the exception of a Monte Carlo simulation of a three-dimensional model of a reticulated-foam packed-bed reactor,[8] at the present time there is no systematic approach available to assimilate a high-density bed of packed solid particles of nonnegligible diameter to a pseudohomogeneous medium with a consistent transport model for electromagnetic energy.[15,16]

Heterogeneous photocatalytic reactions can be carried out with the solid semiconductor, usually titanium dioxide, immobilized on a preferably transparent support in fixed-bed configurations. A typical example of a fixed-bed photocatalytic reactor is that with a packed bed of small spherical beads made of silica (ca. 0.001 m) coated with titanium dioxide. The reactor could have an annular configuration with a tubular UV lamp placed coaxially with the annular space filled with the packing.

The precise modeling of the reactions occurring in this particular reactor cannot be made without an equivalently detailed knowledge of the activation phenomenon corresponding to the first kinetic step. Activation, produced by illumination with light of the appropriate energy, requires a rigorous description of the existing radiation field. The light spatial distribution is the result of two main types of interactions: (i) a mechanism of direct irradiation of a catalytic bead from the lamp and (ii) a mechanism of direct exchange of photons between closely placed beads. This cooperative phenom-

* To whom correspondence should be addressed. Fax: +54 (0)342 4559185. E-mail: acassano@ceride.gov.ar.

10.1021/ie020984w CCC: $27.50
Published on Web 02/21/2004

enon (i.e., the bead-to-bead exchange) is mostly a two-particle event that can be precisely modeled, including absorption, reflection, refraction, and transmission, provided that we have at our disposal a statistical description of the spatial distribution of beads in the packing.

This is so because the structure of the bed is not uniform. One must especially consider that because of the strong radiation absorption properties of the employed semiconductors, particularly in the case of titanium dioxide, photocatalytic packed beds cannot be too thick along the characteristic direction of radiation propagation. Hence, for all practical reactor configurations, wall effects on the packing structure will propagate to a significant part of the existing reaction space between the containing walls that limit the annular space.

To support the radiation-exchange model of a realistic statistical description of the solid structure, two different distribution functions have been obtained: (i) the one-particle distribution function, giving the probability of finding the center of a bead at a given position in space, and (ii) the two-particle distribution function, which tells us the probability of finding a pair of particles close to each other from the knowledge of the distribution function of each particle separately and of the pair of correlation functions.

A thorough discussion of the physical models presented in this work, as well as detailed mathematical derivations, can be found in the Supporting Information of this paper.

The Reactor

The proposed device is an annular packed-bed photocatalytic reactor operating either as a one through or in a partial recycle loop. The reactor packing consists of a bed of silica spheres of $d_p \approx 0.001$ m average diameter, partially or totally covered with a thin film of TiO_2 photocatalyst and confined between concentric cylinders of radii $R_e = 0.050$ m and $R_i = 0.025$ m, respectively, as schematically shown in Figure 1.

The length of the catalytic bed is $L = 0.60$ m, and the annulus inner wall is masked outside this region. Layers of inert spheres (without catalytic coating) extend the packing both from the bottom of its active region downward and from its top end upward. This allows a fully developed flow pattern to reach the catalytic section of the bed and avoids the need for considering end effects in the statistical description of the bed structure.

If needed, for rather slow reactions, the continuous reactor operation in a partial recycle loop allows one to achieve large flow rates per pass without lowering the overall residence time. Larger flow rates amount to larger values of the Reynolds number, defined on the basis of the superficial velocity of the fluid and the diameter of the spheres in the packed bed. In this way, highly turbulent flow regimes can be achieved, minimizing the importance of mass diffusion effects through the film adjacent to the catalytic surface of the spheres. This desirable effect brings about an increasing pressure drop along the reactor axial direction and the possibility of eroding the TiO_2 of the spherical beads as its counterpart.

It is well-known that in annular packed beds with $(D_e - D_i)/d_p > 20$ the two containing walls are far enough apart to act independently and will not simultaneously affect the bead distribution.[17] The annular reactor packing satisfies this condition because $(D_e - D_i)/d_p \approx 25$. In addition to this, the aspect ratio referring to the diameter of the annulus inner wall is $D_i/d_p \approx 50$, sensibly larger than $D_i/d_p \approx 20$, which is considered to be the lower value of the aspect ratio for the wall curvature to have any measurable effect on the bead distribution.[18]

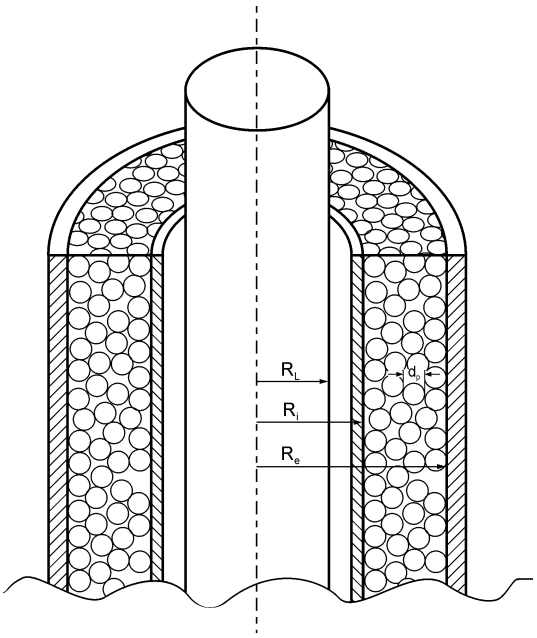

Figure 1. Reactor configuration.

Under these conditions, the annular reactor packing confined between cylindrical walls can be approximated as a slab between parallel-plane surfaces at a distance of $D_e - D_i$ from one another.

Model of the One-Particle Distribution Function

The description of the direct lamp-to-bead exchange requires the knowledge of the distribution of single beads in the packing. A model of the spatial distribution of single spheres in the reactor bed must account for (i) the effect of the reactor walls on the packing structure and (ii) the effect of the volume exclusion between spheres of nonnegligible diameter, propagating the distorsive wall effects deeper inside the packing.

These two effects preclude the possibility of considering the bed as homogeneous and isotropic, at least for sets of structural parameters within the range of practical interest. This is more so because the thickness of an annular photocatalytic reactor employing titanium dioxide as the catalyst is always small.

We denote by $f^{(1)}(\mathbf{r}_1)\, d^{(3)}\mathbf{r}_1$ the probability of a bead having its center contained in the elementary volume $d^{(3)}\mathbf{r}_1$ about the generic position $\mathbf{r}_1$. The function $f^{(1)}(\mathbf{r}_1)$ is the corresponding one-bead distribution function.

Under the conditions discussed in the previous section, allowing one to approximate the annular reactor packing as a slab between parallel-plane surfaces, $f^{(1)}(\mathbf{r}_1)$ is a function of a single variable x_1, running along an axis perpendicular to the slab boundaries. Therefore,

by choosing a unit area perpendicular to the x_1 axis, we may write

$$f^{(1)}(\mathbf{r}_1)\, \mathrm{d}^{(3)}\mathbf{r}_1 = f^{(1)}(x_1)\, \mathrm{d}x_1 \tag{1}$$

where $f^{(1)}(x_1)\, \mathrm{d}x_1$ is the probability of a bead having its center contained in the elementary volume of thickness $\mathrm{d}x_1$ around the location x_1.

A model of the one-particle distribution function has been proposed based on the following physical picture:

(a) There is a layer of beads leaning against each one of the reactor walls, with the bead centers precisely at a distance $x_1 = 1$ from its neighboring wall.

(b) A gap zone without bead centers follows from this layer in the direction toward the inside of the packing. This is a consequence of the volume-exclusion effect of the beads in the first layer upon neighboring inner ones. This gap stretches from $x_1 = 1$ to $x_1 = x_0 > 1$, with x_0 an adjustable parameter depending on the compactness of the packing.

(c) As the distance from the wall increases beyond this gap, the distortion effect of the walls on the packing structure weakens. Successive bead layers become more diffuse until a uniform distribution is asymptotically reached at the core region of the packing.

The proposed model of the one-bead distribution function, fulfilling all of these requirements, is (given in the Supporting Information)

$$f^{(1)}(x_1) = C\delta(x_1-1) + H(x_1-x_0)\, \varphi(x_1) \tag{2}$$

In eq 2, $\delta(x_1-1)$ is the Dirac delta "function", which is zero everywhere, except at $x_1 = 1$, where it is unbounded; $H(x_1-x_0)$ is the Heaviside step function, which is zero for $x_1 - x_0 < 0$ and equals unity for $x_1 - x_0 > 0$; and

$$\varphi(x_1) = n_\infty - n_\infty \mathrm{e}^{-b(x_1-x_0)}\{\cos[a(x_1-x_0)] + (b/a)\sin[a(x_1-x_0)]\}, \quad x_1 > x_0 \tag{3}$$

From this model of the one-bead distribution function, it follows that the corresponding volume fraction of solids is

$$\eta(x_1) = C\pi r_\mathrm{p}{}^3[1-(x_1-1)^2]H(2-x_1)\, H(x_1) + \pi r_\mathrm{p}{}^3 \int_{-1}^{1} \mathrm{d}\zeta(1-\zeta^2)\, \varphi(x-\zeta)\, H[(x_1-\zeta)-x_0] \tag{4}$$

A thorough discussion of the physical model and the detailed derivations of the results in this and in subsequent sections can be found in the Supporting Information of this paper.

Two-Bead Correlation Function

When other possible indirect contributions (like mechanisms involving three or more beads simultaneously) are neglected, the prevailing two-body energy exchange is a short-range phenomenon. This is so because this mechanism involves a "test" particle at the generic position $\mathbf{r}_1$ and those in the shell of nearest neighbors, whose positions are collectively represented by $\mathbf{r}_2$.

The contributions to this indirect exchange mechanism are sketched in Figure 2. A fraction of the total energy reaching the differential area $\mathrm{d}^{(2)}A_1$ on the surface of the bead at the position $\mathbf{r}_1$ comes from beams reflected on differential areas $\mathrm{d}^{(2)}A_2$ of neighboring beads

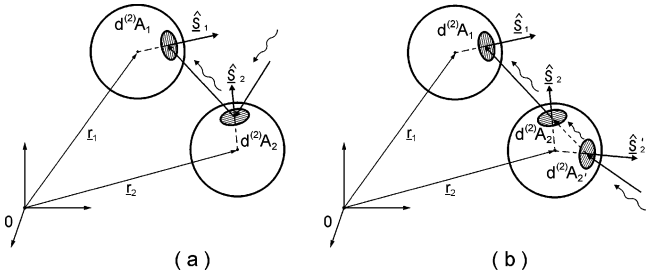

Figure 2. Contributions to the bead-to-bead exchange mechanism: (a) contribution to the total energy reaching the differential surface area $\mathrm{d}^{(2)}A_1$ on the bead at the position $\mathbf{r}_1$, after a reflection on a differential surface area $\mathrm{d}^{(2)}A_2$ of a neighboring bead at the position $\mathbf{r}_2$; (b) contribution due to a beam refracted and partially absorbed by the bead at the position $\mathbf{r}_2$ before reaching the differential surface area $\mathrm{d}^{(2)}A_1$.

at position $\mathbf{r}_2$, as shown in Figure 2a. The rest of the energy reaching the differential area $\mathrm{d}^{(2)}A_1$ by this bead-to-bead mechanism is due to beams refracted and partially absorbed by the other beads at position $\mathbf{r}_2$ around the central bead at $\mathbf{r}_1$. This contribution is sketched in Figure 2b.

The statistical description of the above-described bead-to-bead exchange requires the knowledge of the spatial distribution of a pair of beads. The joint probability distribution $f^{(2)}(\mathbf{r}_1,\mathbf{r}_2)$ of the compound event consisting of particle "1" at $\mathbf{r}_1$ and particle "2" at $\mathbf{r}_2$ can be written in terms of the correlation function $g(\mathbf{r}_1,\mathbf{r}_2)$ defined as follows:

$$f^{(2)}(\mathbf{r}_1,\mathbf{r}_2) \equiv f^{(1)}(\mathbf{r}_1)\, f^{(1)}(\mathbf{r}_2)\, g(\mathbf{r}_1,\mathbf{r}_2) \tag{5}$$

The conditional probability distribution $f^{(2/1)}(\mathbf{r}_2/\mathbf{r}_1)$ that particle "2" be at $\mathbf{r}_2$, given the certain fact that particle "1" is at the position $\mathbf{r}_1$,

$$f^{(2/1)}(\mathbf{r}_2/\mathbf{r}_1) \equiv f^{(2)}(\mathbf{r}_1,\mathbf{r}_2)/f^{(1)}(\mathbf{r}_1) \tag{6}$$

can also be written in terms of $g(\mathbf{r}_1,\mathbf{r}_2)$ as follows:

$$f^{(2/1)}(\mathbf{r}_2/\mathbf{r}_1) = f^{(1)}(\mathbf{r}_2)\, g(\mathbf{r}_1,\mathbf{r}_2) \tag{7}$$

Once again, we will take advantage of the fact that, because of our reactor characteristics, the annular packing confined between cylindrical walls can be approximated as a slab between parallel-plane surfaces. By exploitation of the invariance and symmetry properties of the function $f^{(2)}(\mathbf{r}_1,\mathbf{r}_2)$ arising from this fact, in Appendix I it is shown that the following expression holds:

$$f^{(2)}(\mathbf{r}_1,\mathbf{r}_2) = f^{(2)}(x_1;x_1+\rho\cos\theta) \tag{8}$$

where only the minimum set of independent variables has been retained. The same arguments lead us to conclude that

$$f^{(2/1)}(\mathbf{r}_2/\mathbf{r}_1) = f^{(1)}(x_1+\rho\cos\theta)\, g(x_1;x_1+\rho\cos\theta) \tag{9}$$

All of the surrounding beads effectively participating in the energy exchange with a central "test" particle are contained inside a sphere of radius ρ_nc. Beads located at larger radial distances from the central particle do not contribute effectively in two-body radiation exchange with it. Therefore, both $f^{(2)}(\mathbf{r}_1,\mathbf{r}_2)$ and $g(\mathbf{r}_1,\mathbf{r}_2)$ can

be considered short-range functions that are equal to zero outside a sphere of radius ρ_{nc}.

Two-Bead Correlation Function in Packed Spherical Beads: Physical Background

In a packed bed of rigid spheres, each bead must be in contact with other beads that hold it in its place, thus restraining its motion possibilities. Therefore, the first shell of nearest neighbors in contact with the central particle is, at least, partially built. Its degree of completion will depend, other factors aside, on the "test" particle proximity to a containing wall, which precludes the completion of a compact packing arrangement. Therefore, we may expect that this shell will be completed to a lesser degree for central beads located closer to the walls, where the wall distortion effects on the packing structure are more important than those located in the core region.

The solid volume fraction of a close-packed homogeneous arrangement of rigid beads is $\eta_{CP} = 0.742$. This is the upper bound of η in an infinite, perfectly arranged system without distorting wall effects. On the other hand, the solid-phase behavior is observed for $\eta > \eta_{LS} = 0.47$ in rigid-sphere systems.[19]

As η decreases in the range $\eta_{LS} < \eta < \eta_{CP}$, the spherical beads have their motion possibilities still restrained and collectively behave like an increasingly random, and therefore less compact, solid phase. This behavior is common to all systems of rigid spheres irrespective of the size of the beads, in regions far from their boundaries where the spatial structure is held together only by the interactions between rigid beads.

To propose a model for the two-bead correlation function for our nonisotropic and nonuniform packing, we are going to borrow from statistical mechanics the results obtained for dense isotropic and uniform systems of rigid spheres. To extend these results to our case, we will consider the central particle as if it were embedded in different uniform and isotropic media, each one with a different solid volume fraction η^*. The η^* values are chosen among the actual η values found by surveying the central particle surroundings along every radial direction, as we will see later on.

Abundant experimental results allow us to know with great accuracy the behavior of the pair correlation function in rigid-sphere fluids or in real fluids that approximate the rigid-sphere interaction, like argon or xenon.[19]

In these homogeneous and isotropic systems, with a uniform solid volume fraction η, the pair correlation function depends on the distance between the bead centers, ρ, and not on the particular positions of the spheres. As long as the system of rigid spheres is homogeneous and isotropic, this remains true for all of its possible states: gas, liquid, or solid.

Apart from its dependence on the radial distance ρ, the pair correlation function for a homogeneous and isotropic system of hard spheres only depends on the phase "dimensionless density" η (i.e., on our solid volume fraction).

Because this behavior is a consequence of the singular nature of the hard-sphere interaction, it is shared by all homogeneous and isotropic large collections of rigid spheres behaving as a solid phase, no matter what the bead single diameter could be.

In a finite packing of rigid spheres, a solid system with these characteristics can be approximated by the packing core region if it is far enough from its containing boundaries. In this region, the solid-phase spatial structure is held together only by the interaction forces between beads and is free from the interference of boundary effects.

In this region, the solid-phase spatial structure at a radial distance ρ from an arbitrarily singled-out bead is described by the pair correlation function also depending on η as a parameter. To account explicitly for this dependence, we will adopt the following notation:

$$g(\mathbf{r}_1,\mathbf{r}_2) = g(\rho;\eta) \tag{10}$$

where η is a parameter for each homogeneous and isotropic solid system.

Two-Bead Correlation Function in Packed Spherical Beads: A Mathematical Model

An assembly of randomly packed spheres can represent certain features of the structure of dense simple liquids. For a liquid of rigid spheres, the radial distribution function from statistical mechanics shows the general mathematical form found for randomly packed spheres.[20] However, because the results from statistical theories of classical fluids are not applicable without further considerations to packing densities as high as those of a loose packed bed, outright quantitative agreement cannot be expected.

A large body of numerical simulations has given strong evidence for the adequacy, over an extensive range of parameters, of various approximate theories for the pair correlation function in classical fluids. The simplest of these, and, on the basis of comparisons against numerical simulations, the most satisfactory, is the Percus−Yevick (PY) theory.[19]

A close form of the pair correlation function $g(\rho;\eta)$ for a homogeneous and isotropic fluid of rigid spheres was obtained by Wertheim[21] on the basis of the PY theory. The Wertheim (W) solution behaves satisfactorily beyond the range of η for which the approximations on which the PY theory is based are considered valid. In fact, the W solution is able to approximate results of exact numerical simulations up to $\eta \approx \eta_{LS}$.

Because of the volume-exclusion effect of the central particle on its immediate surroundings, the two-particle correlation function must be zero in the interval $0 < \rho < 2$, irrespective of whether the system is homogeneous and isotropic or not. Beyond $\rho = 2$, the W analytical solution for the case of an infinite, isotropic medium is expressed in the form

$$g(\rho;\eta) = \sum_{n=1}^{\infty} g_n(\rho;\eta) \tag{11}$$

where the dependence of the pair correlation function on the uniform solid volume fraction has been made explicit.

A generic nth term, $g_n(\rho;\eta)$ in eq 11, behaves as follows:

$$g_n(\rho;\eta) = 0; \quad \rho < 2n \text{ or } \rho > 2n \tag{12a}$$

$$g_n(\rho;\eta) > 0; \quad 2n < \rho < 2n + 2 \tag{12b}$$

for $n = 1, 2, \ldots, \infty$. The interpretation of eq 12a,b is that, for a given ρ, only one term of eq 11 is different from zero, namely, the one whose label n satisfies the

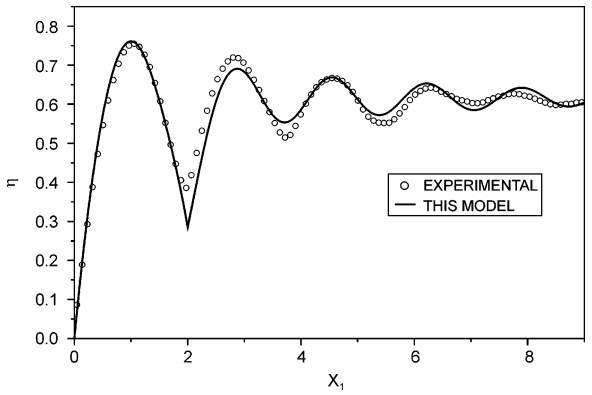

Figure 3. Comparison of experimental, η_{exp}, against model predicted, η_{th}, solid volume fractions as functions of the distance from the wall with the parameter values of Table 1.

condition $2n < \rho < 2n + 2$, with n an integer number. As a result of this, eq 11 offers a description of $g(\rho;\eta)$ in terms of concentric layers, with each one relieving the preceding layer as ρ increases in the interval $2 < \rho < \infty$.

Except for its core region far from the containing walls, our packing differs from those systems for which the W pair correlation function has been derived in that it is neither uniform nor isotropic. Besides, the solid volume fraction in the core packing region is expected to be $\eta_\infty \approx 0.62$, corresponding to the solid-phase region of an isotropic and homogeneous system of rigid spheres and halfway between η_{LS} and η_{CP}. The W close expression of $g(\rho;\eta)$ is not applicable as a predicting tool to packing densities as high as these. Outside the range of η where the theory is valid, the W mathematical form of the pair correlation will be adopted as a sensible expression on which to lay a model of the first layer surrounding a central bead in the narrow band of $2.0 < \rho < \rho_{nc}$ and for the dimensionless densities η of interest here.

If we choose the test particle at positions increasingly closer to the walls, its surroundings become more and more structured as the wall effects on the bead spatial distribution become stronger. By sampling a spherical couch of radius ρ, with $2 < \rho < \rho_{nc}$, surrounding the test particle, we will find different values of η depending on the radial direction chosen, as can be seen in Figure 3 for $x = x_1 + \rho \cos\theta \leq 10$.

As part of our model, we will assume that the exclusion effect of the central bead on its nearest neighbors propagates along each direction through its nonhomogeneous environment, as it would have done in a hypothetical homogeneous and isotropic packing with a solid volume fraction η^*. The η^* values are chosen among the actual η values found along every radial direction from the test particle. Therefore, η^* will depend on every particular direction chosen.

The value of η^* for the direction of search, θ, will be chosen as the local value of η in the structured medium, taken at the halfway position between the center of the test bead, x_1, and that of its closest neighbor, $x_1 + \rho \cos\theta$.

With this choice, η^* will depend on the direction considered as follows:

$$\eta^* = \eta\left(x_1 + \frac{1}{2}\rho\cos\theta\right); \quad 2 < \rho < \rho_{nc}; \quad 0 < \theta < \pi \qquad (13)$$

We will assume that the W expression of the pair correlation function for homogeneous and isotropic fluids is applicable to describe the first surrounding layer around a central particle in a packed bed, as long as we use the direction-dependent η^* as the dimensionless concentration.

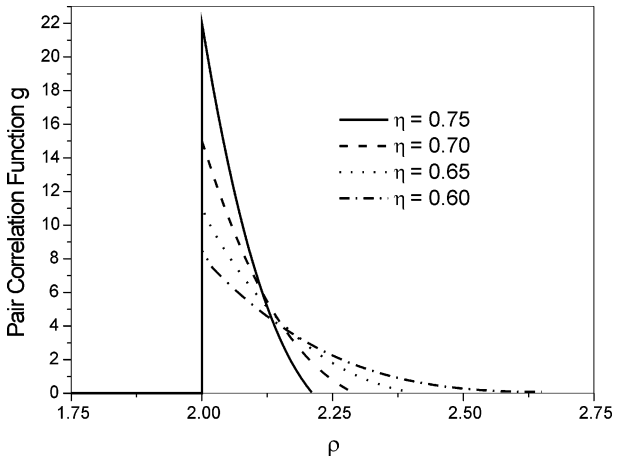

Figure 4. Pair correlation function $g(\rho;\eta)$ as a function of ρ for different value of η.

In previous sections, we have argued that only those pairs of beads with distances between centers, ρ, in the interval $2 < \rho < \rho_{nc} < \rho_{cp} = 3.266$ are provisionally considered to account for the bead-to-bead energy exchange mechanism. Therefore, for our purposes in this work, only the first layer contribution to the W expression of $g(\rho;\eta^*)$ will be retained.

$$g(\rho;\eta^*) = g_1(\rho;\eta^*) \qquad (14)$$

The expression of $g_1(\rho;\eta)$ according to the W solution is given in Appendix II, and its profiles for different values of η are shown in Figure 4. The sharp peak observed at $\rho = 2$ corresponds to the beads in contact with the central one. It is followed by a steep downward slope until $g_1(\rho;\eta^*)$ reaches a local minimum, as shown in Figure 4. For values of $\rho > \rho_{min}$, the local minimum is overshot, the probability for a second layer begins to build up, and $g(\rho;\eta^*)$ increases up to a local maximum.

A spherical volume with radius $\rho = \rho_{min}$ will enclose the entire first couch of beads surrounding the central particle. Therefore, the choice of $\rho_{nc} \approx \rho_{min}$ appears as the natural one. With this choice, the values of $g(\rho;\eta)$ in the narrower but more realistic interval $2 < \rho < \rho_{nc} \approx \rho_{min}$ correspond to the statistical description of the first shell of neighboring particles.

For the largest values of the parameter η^*, it may happen that the downward slope following the sharp peak at $\rho = 2$ is so steep that $g(\rho_{min};\eta^*)$ reaches a relatively small and negative value. This unphysical situation is corrected by requiring that $g(\rho;\eta)$ always be positive or zero.

With this model of the pair correlation function in the packed bead and the symmetry considerations made in the Supporting Inforamtion of this paper, eq 5 may be written as

$$f^{(2)}(\mathbf{r}_1,\mathbf{r}_2) \approx f^{(1)}(\mathbf{r}_1)\, f^{(1)}(\mathbf{r}_2)\, g_1(\rho;\eta^*) \qquad (15)$$

where $2 < \rho < \rho_{nc}$ and $0 < \theta < \pi$.

The conditional probability distribution $f^{(2/1)}(\mathbf{r}_2/\mathbf{r}_1)$, defined in eq 7, may also be written in terms of $g(\rho;\eta^*)$:

$$f^{(2/1)}(\mathbf{r}_2/\mathbf{r}_1) \approx f^{(1)}(\mathbf{r}_2)\, g_1(\rho;\eta^*) \qquad (16)$$

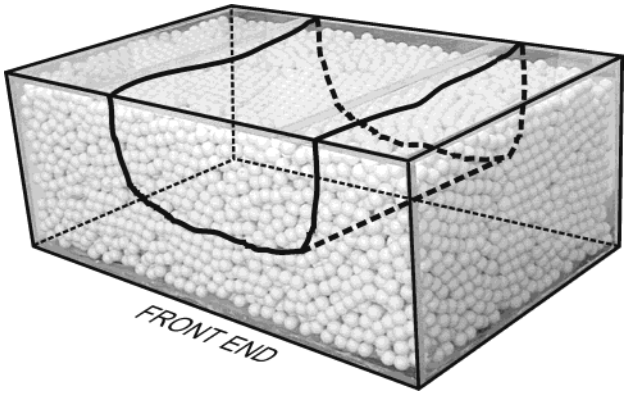

Figure 5. Scaled-up prototype consisting of a rectangular acrylic box filled at random with glucose spheres of 10^{-2} m diameter. The bed structure was determined by computed tomography.

Equation 16 completes our model for the statistical description of the packed-bed structure based on the probability of occurrence of single beads and of pairs of beads.

In the following sections of this paper, we will describe the direct experimental measurement of both the one- and two-bead distribution functions, as well as that of the solid volume fraction. These results were obtained by means of computer tomography experiments performed on an up-scaled physical model of the packed bed. The model adjustable parameters $\{C; n_\infty; a; b; x_0\}$ will be regressed from these experimental data.

Experimental Validation of the Model

The statistical model of the annular packing bed has been tested on a scaled-up prototype constructed so that it retains the distinctive characteristics and assumptions made on the bench-scale packed-bed reactor. The three-dimensional structure of the prototype packing has been determined using computerized tomography.

The prototype, sketched in Figure 5, consists of a rectangular acrylic box filled at random loose-packed conditions (i.e., packing material poured without tamping)[20,22,23] with glucose spheres of average diameter $d_p = 1.089 \times 10^{-2}$ m. Glucose was chosen as the bead material for convenience because it resembles the composition of the bodily tissues more closely than the original silica beads, a crucial aspect to consider given the fact that the bed structure was determined by computerized tomography using a Elscint (Picker) model 98 instrument for human diagnosis.

The sizes of the glucose beads are about 10 times larger than the silica ones to reduce the error in the measurements of the diameters of the virtual circular cuts resulting from the intersection of the spheres and the plane wiped by the scanning beam.

The prototype meets the conditions necessary for the front and back containing walls to act independently, so that they will not simultaneously affect the bead distribution at any point in the bed.[17]

According to the model of Martin,[18] wall effects on the packing structure die out within a 10-bead diameter distance from the particular wall considered. The shape and size of the box have been chosen so that an upper central region in the packing of about 20-bead-diameter width and 6-bead-diameter depth, free from distortions from the lateral walls as well as from the bottom, could be cut out as the working sample, which is sketched in Figure 5. In this central core region, the only distortions remaining are those due to the front and back walls, whose impact on the spatial distribution of single beads and of pairs of beads is precisely the objective of the present study.

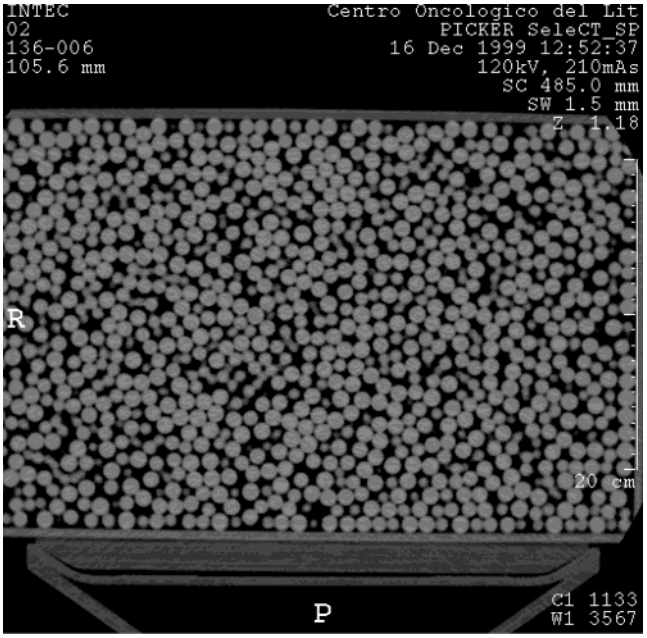

Figure 6. One among seven plane virtual cuts made with the tomography instrument across the core region.

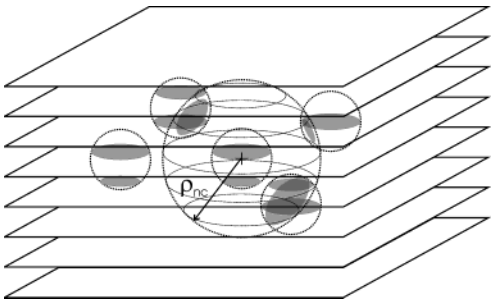

Figure 7. Intersections of beads and virtual cutting planes showing shadowy circular intersections with diameters equal to or smaller than d_p. Two circular traces on contiguous planes aligned on the same vertical line belong to the same bead. The ball of radius ρ_{nc} includes the couch of nearest neighbors surrounding the chosen central bead.

A total of seven virtual plane cuts, such as the one shown in Figure 6, were made with the tomography instrument in the core region. The successive plane cuts were made at an average distance of 0.0056 m from each other. Actually, every plane cut is a slab of approximately 1.0×10^{-3} m thickness. Except for very unlikely local situations, two contiguous planes cut each bead in the sample region, as is depicted in Figure 7.

The intersection of a bead by a plane produces a circular trace on it, with a diameter that is either equal to or smaller than d_p. When the centers of two circular traces on contiguous planes are aligned on the same vertical line, we can ensure that they belong to the same bead and that the bead center will be in the space between these two planes. The possibility of two circular traces on contiguous planes, aligned on the same vertical and belonging to two different beads, is dismissed as a very unlikely event.

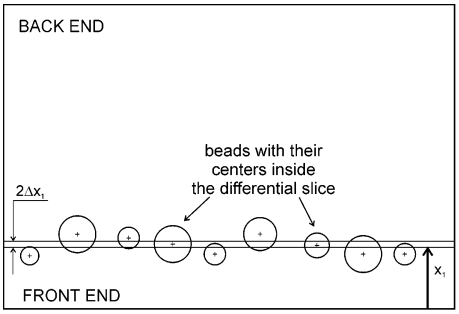

Figure 8. Sketch of the $f^{(1)}(x_1)$ construction procedure based on the detailed structure of the packing.

On the basis of two concentric circular traces on contiguous cuts and their respective diameters, the spatial location of each bead can be determined. Because the average bead radius is known beforehand, a vertical coordinate value can be assigned to the bead center between the two planes. This procedure allows one to determine the spatial location of every bead because the coordinates on the cutting planes can be directly measured. Therefore, the spatial structure of the entire sample core can be expressed in terms of the positions of the centers of all beads by processing the images of the sequence of cuts.

Experimental Construction of the One-Bead Distribution Function

Once the spatial structure of the entire core sample has been reconstructed as discussed in the previous section, we may consider a transversal virtual slice of differential width, parallel to both the front and back walls, as sketched in Figure 8. We may think of this slice as moving from a position by the front wall toward the back wall by a small stretch at a time.

The moving differential slice incorporates new bead centers while leaving behind others, according to the uneven distribution it finds along the direction of its virtual motion, until half of the distance between the front and back walls is entirely swept. At every new position, the number of bead centers inside the slice is recorded automatically and accumulated to previous counts.

Then, this counting procedure is repeated, starting from the back wall up to the half-distance between the two confining walls. The cumulative counts registered at equal distance, x_1, from each one of the walls are added up to give $N_{exp}(x_1)$. This experimental procedure approximates the integral function

$$\frac{N_{exp}}{2A_T} = \int_0^{x_1} dx\, f^{(1)}(x); \quad 0 < x_1 < x_M \tag{17}$$

where A_T is the cross-sectional area of the working sample; $x_M = D/2d_p$ is the position of the midpoint between the two confining walls; and the factor of 2 in the denominator of the left-hand side of eq 17 takes into account the fact that we are accumulating, on the average, a number of beads 2-fold as large as the one corresponding to each position x_1 in the interval $0 < x_1 < x_M$.

Substitution of eqs 2 and 3 into eq 17, followed by integration, gives the theoretical explicit form of the cumulative function $N_{th}(x_1)$ in terms of the set of parameters $\{C; n_\infty; a; b; x_0\}$

$$\frac{N_{th}}{2A_T} = \left[C - \frac{2bn_\infty}{a^2+b^2}\right] + n_\infty\left\{(x_1 - x_0) - \frac{e^{-b(x_1-x_0)}}{a(a^2+b^2)}[(a^2-b^2)\sin a(x_1-x_0) - 2ab\cos a(x_1-x_0)]\right\} \tag{18}$$

which is valid for $x_1 > x_0$.

For $x_1 \gg x_0$, eq 18 tends to the linear expression

$$\frac{N_{th}}{2A_T} = \left[C - \frac{2bn_\infty}{a^2+b^2}\right] + n_\infty(x_1 - x_0) \tag{19}$$

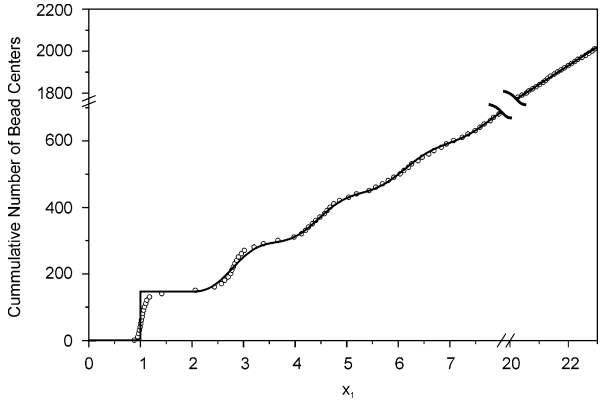

Figure 9. Comparison of experimental, N_{exp}, against model predicted, N_{th}, cumulative number of bead centers as functions of the distance from the wall.

Table 1. Set of Values of the Model Parameters Obtained by Nonlinear Regression of the Experimental Data of Figure 9, Using the Model Equation (18)

parameter	value	parameter	value
C (beads/m^3)	1.50×10^6	n_∞ (beads/m^3)	9.11×10^5
a	3.76	x_0	1.94
b	0.21		

The experimental cumulative number of beads, N_{exp}, as a function of the distance to the wall, x_1, is compared against the theoretical profile in Figure 9 for the set of parameters of Table 1. The agreement between the model predictions and experiments is quite satisfactory over the entire range of x_1. Besides, the linear asymptotic form of eq 19 with a slope equal to n_∞ is confirmed by the experimental results. The profile of $f^{(1)}(x_1)$ obtained from eqs 2 and 3, with the parameters of Table 1, is shown in Figure 10. The vertical spike at $x_1 = 1$ is an icon to denote the Dirac delta function of eq 2.

Experimental Construction of the Volume Fraction of Solids

To construct the local volume fraction of solids, we may address our attention to the virtual experiment of the previous section, which has been devised to determine the one-bead distribution function. As before, we may consider a transversal virtual slice of differential width Δx_1, at a distance x_1 from either the front or the back wall, as sketched in Figure 8. This slice is assumed to be continuously moving toward the midpoint between the front and back walls. At the midpoint region

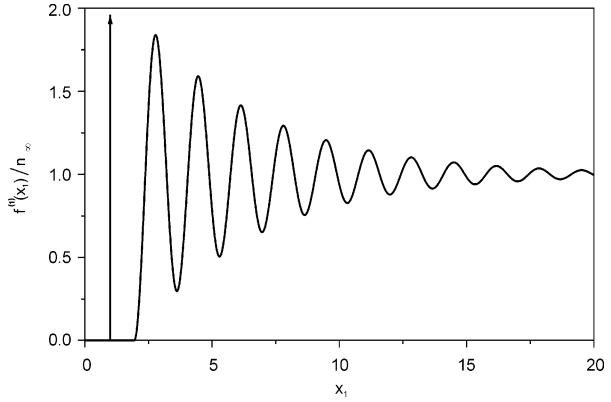

Figure 10. Profile of $f^{(1)}(x_1)$ obtained from eq 2 with the parameters of Table 1. The vertical spike at $x_1 = 1$ is an icon to denote the Dirac delta function.

between the containing walls, n_∞ can be related to the solid volume fraction, η_∞, in a simple way:

$$\eta_\infty = v_p n_\infty \tag{20}$$

Considering that in our prototype $v_p = 6.76 \times 10^{-7}$ m^3/bead and that from the results in Table 1 $n_\infty = 9.11 \times 10^5$ beads/m^3, the asymptotic value of the volume fraction of solids far from either wall is $\eta_\infty = 0.616$. This value corresponds to an intermediate situation between the loose random packing ($\eta_\infty = 0.60$) and the dense random packing ($\eta_\infty = 0.63$).[20]

As can be seen in Figure 8, the beads contributing to the solid volume fraction at a distance of $x_1 < x_M$ from either one of the two containing walls are those with centers at a generic position y_j from the same wall, such that $x_1 - 1 < y_j < x_1 + 1$.

Assuming that there is a bead at the generic position y_j, its cylindrical volume of intersection with the differential slab at x_1 is

$$\delta A(x_1,y_j) = \pi r_p^2[1 - (x_1 - y_j)^2]\Delta x_1; \quad x_1 - 1 < y_j < x_1 + 1 \tag{21}$$

The total volume of solids $\delta V_M(x_1)$ contained in two elementary slabs, each one at a distance x_1 from its nearest wall, can be calculated by adding up the contributions from all of the beads found at positions y_j, which are at a distance of less than unity away from x_1:

$$\delta V_M(x_1) = \sum_j \delta A(x_1,y_j) \tag{22}$$

The experimental local volume fraction of solids, $\eta_{exp}(x_1)$, is obtained as the ratio of the volume of solids in the sampling slabs, $\delta V_M(x_1)$, to the volume of the slabs, $2A_T\Delta x_1$:

$$\eta_{exp}(x_1) = \frac{\delta V_M(x_1)}{2A_T\Delta x_1} \tag{23}$$

In Figure 3, the values of $\eta_{exp}(x_1)$ are compared with those of $\eta_{th}(x_1)$ predicted with the model equation (4) and the parameter values of Table 1. The agreement is remarkable, especially in the region of $x_1 < 4$, where the effects of the confining walls are strong and the bead layers are highly ordered.

Experimental Construction of the Conditional Distribution Function

The conditional probability distribution $f^{(2/1)}$ that bead 2 is at $x_2 = x_1 + \rho \cos\theta$ given the fact that bead 1 is at the position x_1 will only depend on the central particle distance to its nearest wall, x_1, and on the projection of the relative distance between the two particles on the x_1 axis, $\rho \cos\theta$, in the form of

$$f^{(2/1)}(\mathbf{r}_2/\mathbf{r}_1) = f^{(1)}(x_1+\rho\cos\theta)\, g_1(\rho;\eta^*) \tag{24}$$

as follows from eqs 7, 9, and 16.

To construct $f^{(2/1)}$ experimentally, we have to calculate the number of beads per unit volume that can be found in the average, at a distance $\rho > 2$ along the direction μ from a central bead, located at a distance x_1 from any of the two end walls.

Once the spatial structure of the entire sample core is known, we consider again a slice of differential thickness, parallel to both the front and back walls and located at a distance x_1 from each of them at a time. To determine the $f^{(2/1)}$ conditional distribution function, we start by singling out a central or "test" particle (bead "1"), one among the particles with its center in the slice at the chosen position x_1.

Let us assume that the position of the picked central bead in the three-dimensional space is $[(x_i, y_i, z_i); x_1 - \Delta x_1 < x_i < x_1 + \Delta x_1]$, where Δx_1 is the slab half-width. Then we search for beads with centers in the spherical layer of radius within the small interval $[(\rho - \Delta\rho, \rho + \Delta\rho); \rho > 2.0]$ surrounding the central bead. For this, we check for every other bead at a generic position (x_j, y_j, z_j), different from that of the central one, whether the condition $\rho - \Delta\rho < \rho_{ij} < \rho + \Delta\rho$ where $\rho > 2.0$ and

$$\rho_{ij} = [(x_j - x_i)^2 + (y_j - y_i)^2 + (z_j - z_i)^2]^{1/2} \tag{25}$$

is satisfied or not. When it is satisfied, we consider that bead "2" at (x_j, y_j, z_j) has its center at a distance ρ from the central bead, except for the small tolerance $(2\Delta\rho)$. We are now in conditions to compute the corresponding value of $\cos\theta$ for the considered (i, j) pair as follows:

$$\mu_{ji} = -\cos\theta_{ji} = \frac{(x_j - x_i)}{\rho_{ij}}; \quad -1 < \mu_{ji} < 1; \quad 0 < \theta < \pi \tag{26}$$

A one-dimensional grid of equally spaced values of μ in the interval $-1 < \mu_{ji} < 1$ is defined. For a given value of ρ, the values of μ_{ji} calculated from eq 26 very unlikely will coincide with one of the values of μ corresponding to a node in the grid. Let us assume that the value μ_{ji} falls between the grid contiguous values μ_n and μ_{n+1}; i.e., $\mu_n < \mu_{ji} < \mu_{n+1}$. In this case, the surrounding bead is partitioned into two contributions:

$$w_n(j,i) = \frac{\mu_{n+1} - \mu_{ji}}{\mu_{n+1} - \mu_n} = \frac{\mu_{n+1} - \mu_{ji}}{\Delta\mu} \tag{27a}$$

and

$$w_{n+1}(j,i) = 1 - w_n(j,i) \tag{27b}$$

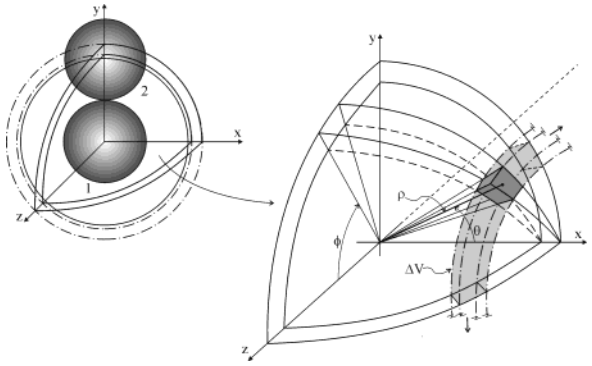

Figure 11. ΔV is the μ-independent elementary volume containing the beads accumulated at a distance ρ from each one of the $n_1(x_1)$ central beads, along any of the directions μ_n, $n = 1, 2, ..., N + 1$.

In eq 27a, $\Delta\mu$ is the constant incremental value of μ between contiguous nodes in the one-dimensional grid.

The $w_n(j,i)$ contribution is assigned to the μ_n node, while the $w_{n+1}(j,i)$ contribution is assigned to the μ_{n+1} node.

Then, for the same given value of ρ, we repeat the search for beads with centers at the generic position (x_j, y_j, z_j) in the spherical layer of radius in the small interval $[(\rho - \Delta\rho, \rho + \Delta\rho); \rho > 2.0]$ surrounding the same central bead at the position $[(x_i, y_i, z_i); x_1 - \Delta x_1 < x_i < x_1 + \Delta x_1]$, until the possibilities are exhausted. The way of assigning fractions of beads to the nodes of the μ grid remains the same.

At this point we have experimentally established how the beads at a distance ρ from a central bead at $[(x_i, y_i, z_i); x_1 - \Delta x_1 < x_i < x_1 + \Delta x_1]$ are distributed according to the directional μ variable.

The procedure is repeated considering every bead in the virtual slice at a distance x_1 from either the front or the back wall as the central particle, and in each case the fractions of each bead are assigned to the nodes of the μ grid and accumulated in them.

At the end of this stage of the calculations, we know (i) the total number of central beads, $n_1(x_1)$, in the two virtual slices at a distance x_1 from either the front or the back wall, respectively, and (ii) the total number of beads surrounding the central ones at a distance ρ, distributed along the μ variable by accumulation of bead fractions in the nodes of the μ grid, $n_2(x_1 - \rho\mu_n)$, $n = 1, 2, ..., N + 1$, where N is the number of intervals in the μ grid.

The average number of surrounding beads per unit volume at a distance ρ from a generic central bead at the position x_1 can be calculated for every μ direction as follows:

$$f_{\text{exp}}^{(2/1)}(x_1 - \rho\mu_n/x_1) = \frac{1}{\Delta V}\frac{n_2(x_1 - \rho\mu_n)}{n_1(x_1)}; \quad n = 1, 2, ..., N + 1 \tag{28}$$

where (as is shown in Figure 11)

$$\Delta V = \int_0^{2\pi} d\phi \int_{\mu_n - \Delta\mu/2}^{\mu_n + \Delta\mu/2} d\mu \int_{\rho - \Delta\rho}^{\rho + \Delta\rho} d\rho\, \rho^2 = \left(\frac{4\pi}{3}\right)(2\rho^2 + \Delta\rho^2)\Delta\rho\Delta\mu \tag{29}$$

is the μ-independent elementary volume containing the beads accumulated at a distance ρ from each one of the $n_1(x_1)$ central beads, along any of the directions μ_n, $n = 1, 2, ..., N + 1$.

The procedure is be repeated for different positions x_1, symmetrical with respect to the midpoint x_M.

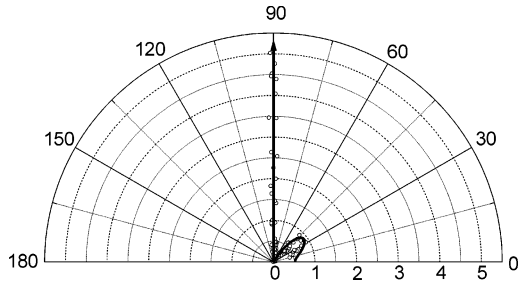

Figure 12. Conditional probability $f^{(2/1)}$ represented as the vector radius in polar coordinates, with the $\theta = 0$ direction collinear with the x_1 axis. The central bead is resting against the confining wall (i.e., $x_1 = 1$) and the surrounding beads are in contact with it (i.e., $\rho = 2$). The experimental points are represented with open circles, while the profile represented by the solid line is the model prediction. The average number of surrounding beads per unit volume at a distance $\rho = 2$ from a central bead, for every μ direction, has been averaged over 90 central beads found at the position x_1.

Comparison of the Model-Predicted Conditional Distribution Function against Experiments

In this section, the values of the conditional probability distribution $f_{\text{exp}}^{(2/1)}$ are compared with those of $f_{\text{th}}^{(2/1)}$ predicted with the model equation (24) and the parameter values of Table 1 for the central bead at different distances x_1 from the nearest wall of our prototype.

Figure 12 corresponds to the case in which the central bead is resting against the confining wall (i.e., $x_1 = 1$) and the surrounding beads are in contact with it (i.e., $\rho = 2$). The conditional probability $f^{(2/1)}$ is represented as the vector radius in polar coordinates, with the $\theta = 0$ direction collinear with the x_1 axis. The experimental points are represented with open circles, while the profile represented by the solid line is the model prediction.

This representation remains invariant under an arbitrary revolution around the $\theta = 0$ direction. The average number of surrounding beads per unit volume at a distance $\rho = 2$ from a central bead, for every μ direction, has been averaged over the local structure around each one of a group of the 90 central beads found at positions $[(x_i, y_i, z_i); x_1 - \Delta x_1 < x_i < x_1 + \Delta x_1]$.

The experimental points gathered along the $\theta = 90°$ axis are remarkably close to what, according to the model, should be the Dirac delta "function", pictorially represented in this figure with a vertical spike. This accounts for the fact that there certainly are neighboring beads in contact with the central one and, at the same time, resting against the wall.

There are no bead centers found in the interval $60 < \theta < 90$, while a local maximum of $f^{((2/1)}$ occurs at $\theta \approx 37°$, corresponding to those beads on the second layer trying to fit in the interstices between the beads of the first layer. For a more detailed discussion of the results, the reader is referred to the Supporting Information of this paper.

Parts a−c of Figure 13 correspond to the case in which the central bead is at the distance $x_1 = 2.775$ from the confining walls. The number of surrounding beads per unit volume at three different distances of $\rho = 2.0, 2.1,$

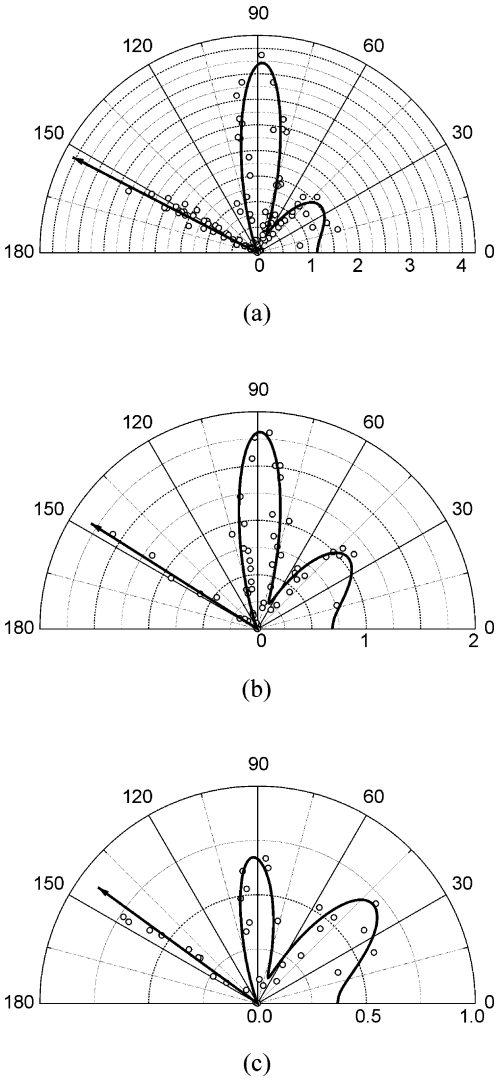

Figure 13. (a) Conditional probability $f^{(2/1)}$ represented as in Figure 12. Every bead at the distance $x_1 = 2.775$ from the wall is chosen as "the" central bead, and the surrounding beads are in contact with it (i.e., $\rho = 2$). The experimental points are represented with open circles, while the profile represented by the solid line is the model prediction. The average number of surrounding beads per unit volume at a distance $\rho = 2$ from the central bead, for every μ direction, has been averaged over 54 central beads found about the position x_1. (b) Same comments as those in Figure 12, except that the surrounding beads are close to the central one but not strictly in contact with it (i.e., $\rho = 2.1$). (c) Same comments as those in Figure 12, except that the surrounding beads are a bit farther from the central one (i.e., $\rho = 2.2$).

and 2.2 from the central one, for every μ direction, has been averaged over the local structures surrounding each one of the 54 central beads found at positions $[(x_i, y_i, z_i); x_1 - \Delta x_1 < x_i < x_1 + \Delta x_1]$.

In Figure 13a, the surrounding beads are in contact with the central particle (i.e., $\rho = 2$). The experimental points gathered along the $\theta = 152.6°$ vector radius are close to what in our model should be the Dirac delta "function", pictorially represented in this figure with a tilted spike. This delta "function" should be zero everywhere, except for the θ angle satisfying the condition

$$x_2 = 1 = x_1 + \rho \cos \theta \qquad (30)$$

for the given values of $\rho = 2$ and $x_1 = 2.775$, where it becomes unbounded. This accounts for the fact that there certainly are neighboring beads in contact with the central one and, at the same time, they belong to the first layer resting against the wall ($x_2 = 1$), while the central bead does not ($x_1 > 1$).

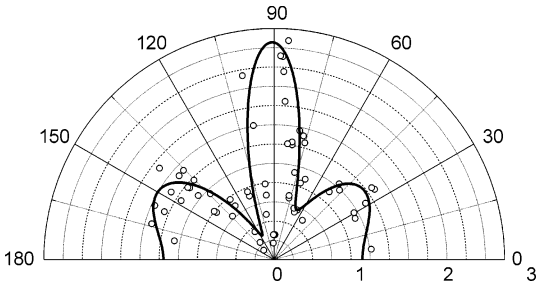

Figure 14. Conditional probability $f^{(2/1)}$ represented as before. Every bead at the distance $x_1 = 4.5$ from the wall that has been chosen is chosen at a time as "the" central bead, and the surrounding beads are in contact with it (i.e., $\rho = 2$). The average number of surrounding beads per unit volume at a distance $\rho = 2$ from the central bead, for every μ direction, has been averaged over the 38 central beads found about the position x_1.

The local maximum of $f^{(2/1)}$ at $\theta = 88.5°$ reveals the existence of a fairly well structured second layer at a distance a bit larger than $x_1 \approx 2.775$ from the wall. Another local maximum of $f^{(2/1)}$ occurs at $\theta \approx 35.3°$, corresponding to those beads of the less structured third layer trying to fill the interstices between the beads in the fairly well-defined second layer.

Parts b and c of Figure 13 correspond to cases where the surrounding beads, although at positions close to the central particle, are not strictly in contact with it. The physical meaning of the profiles is similar to that already discussed for Figure 13a. However, it should be stressed that, as predicted by the model and confirmed by experiments, $f^{(2/1)}$ decays sharply with small increases of the radial distance ρ and that the relative importance of the local minima changes in a very noticeable fashion with small changes in ρ.

Figure 14 corresponds to the case where the "test" particle is located at a radial position $x_1 = 4.5$ from the wall, where the effect of the confining wall on the packing structure is still important.

Considering the $\rho = 2$ contour of Figure 14, we can conclude that the difference between local maxima and minima is less pronounced than those for positions closer to the wall, anticipating the limit circular shapes we expect to find in the homogeneous core region of the packing. The average number of surrounding beads per unit volume at a distance $\rho = 2$ from a central bead, for every μ direction, has been averaged over the local structure around each one of a group of 38 central beads found at positions $[(x_i, y_i, z_i); x_1 - \Delta x_1 < x_i < x_1 + \Delta x_1]$.

The results predicted with the model follow satisfactorily the highly structured shape of the experimental profiles with the central bead at different locations, whether the surrounding particles were in contact with it or not.

Model Parameters and the Bead Radius

The statistical model developed for the description of the spatial structure of a packed bed of spherical-like particles in terms of one- and two-bead distribution functions has been checked against experimental data taken from a scaled-up prototype made of spheres larger than the ones in the packing of our bench-scale reactor.

Although the dimensionless parameters of Table 1 are valid in both cases, the values of n_∞ and C depend on

Table 2. Set of Values of the Model Parameters for the Packing of the Bench-Scale Reactor

parameter	value	parameter	value
C (beads/m^3)	1.93×10^9	n_∞ (beads/m^3)	1.175×10^7
a	3.76	x_0	1.94
b	0.21		

the averaged radius of the spheres of the prototype packing and should be rescaled to be used in our bench-scale reactor.

The packing of the prototype and that of the reactor are both loose random packings and must show the same η_∞ values. From eq 20, this condition can be written as

$$\eta_\infty = \left(\frac{4\pi}{3}\right) r_p{}^3 n_\infty = \left(\frac{4\pi}{3}\right)(r'_p)^3 n'_\infty \tag{31}$$

From the second equality of eq 31, we can change from n'_∞ to n_∞ as follows:

$$n_\infty = \left(\frac{r'_p}{r_p}\right)^3 n'_\infty \tag{32}$$

On the same basis, we can claim that the packing of the prototype and that of the reactor must show the same $\eta(1)$ values. Substitution of $x_1 = 1$ in eq 4 gives

$$\eta(1) = \pi r_p{}^3 C + \pi r_p{}^3 \int_{-1}^{1-x_0} d\zeta (1-\zeta^2)\, \varphi(1-\zeta); \quad 0 < x_0 < 2 \tag{33a}$$

$$\eta(1) = \pi r_p{}^3 C; \quad 2 < x_0 \tag{33b}$$

Considering that the integral in the second term on the right-hand side of eq 33a is proportional to n_∞, that term as a whole must remain unchanged for different values of r_p. Therefore, either from eq 33a or from eq 33b, we reach the following conclusion:

$$C = \left(\frac{r'_p}{r_p}\right)^3 C' \tag{34}$$

Choosing the primed parameters as those of the prototype and considering that $(r'_p/r_p)^3 = 1.29 \times 10^3$, we have the parameter set of Table 2, which is valid in the case of the packing of our bench-scale reactor. Equations 32 and 34 are not restricted to a particular ratio of bead radii and are as general as the model for the one- and two-bead distribution functions presented in this paper.

Equations 32 and 34 are valid to scale the parameters n_∞ and C to any other loose random packing of different bead radii.

Conclusions

The statistical model developed for the description of the spatial structure of a packed bed of spherical-like particles in terms of one- and two-bead distribution functions proposed in this paper is the first step toward the full modeling of the radiation field in an annular photocatalytic reactor, mainly where the interaction between the radiation field and the packed bed is concerned.

The model has been validated against tomography experiments on an up-scaled prototype, whose three-dimensional structure of its loose random packing have been digitized. On the basis of this three-dimensional structure, the experimental versions of $f^{(1)}$, η, and $f^{(2/1)}$ could be constructed without mediating models. Then the parameters of the proposed statistical model could be determined by nonlinear regression.

The agreement between the functions $f^{(1)}_{exp}$, η_{exp}, and $f^{(2/1)}_{exp}$, constructed experimentally, and their counterparts $f^{(1)}_{th}$, η_{th}, and $f^{(2/1)}_{th}$, predicted with the model equations and the set of regressed model parameters, is remarkable despite the highly structured shapes of their profiles.

Exact relationships have been established to scale those model parameters bearing dimensions, to packings of different bead radii; i.e., the obtained results are of general application.

Acknowledgment

Thanks are given to Universidad Nacional del Litoral [CAI+D 96-0017-120 and Project 6 (Program N*o*. 39)], FONCYT (BID 802/OC-AR: PID 95-022, PICT 97-13-00000-01209, and PICT 2000-14-10055), and CONICET (PIP 98-0205) for financial help. We thank J. Romero Acuña M.D., of the Centro Oncológico del Litoral, for giving us free access to the tomography apparatus. The assistance of Héctor Mercke, Daniel Paternó, and Cristián Dagatti with the image processing and drawings, as well as that of Graciela Ferreyra Ch.Eng., in the construction of the scaled-up prototype, is grateful appreciated. The permanent financial assistance of Universidad Nacional del Litoral and CONICET is gratefully acknowledged.

Appendix I

Under the conditions discussed in the main text that allow one to approximate the annular reactor packing as a slab between parallel-plane surfaces, the function $f^{(2)}(\mathbf{r}_1,\mathbf{r}_2)$ must remain invariant when the position vectors $\mathbf{r}_1$ and $\mathbf{r}_2$ are displaced by the same arbitrary vector $\mathbf{r}_0$, parallel to the packing-plane boundaries; i.e.,

$$f^{(2)}(\mathbf{r}_1,\mathbf{r}_2) = f^{(2)}(\mathbf{r}_1+\mathbf{r}_0;\mathbf{r}_2+\mathbf{r}_0) = f^{(2)}(x_1,y_1+y_0,z_1+z_0;x_2,y_2+y_0,z_2+z_0) \tag{I.1}$$

Because of the arbitrariness on $\mathbf{r}_0$, we may choose $y_0 = -y_1$ and $z_0 = -z_1$ to give

$$f^{(2)}(\mathbf{r}_1,\mathbf{r}_2) = f^{(2)}(x_1;x_2,y_2-y_1,z_2-z_1) \tag{I.2}$$

Let us introduce a spherical coordinate system (ρ, θ, ϕ) centered at (x_1, y_1, z_1), with its $\theta = 0$ axis parallel to the x_1 axis of the original rectangular system, such that

$$x_2 - x_1 = \rho \cos\theta \tag{I.3}$$

$$y_2 - y_1 = \rho \sin\theta \cos\phi \tag{I.4}$$

$$z_2 - z_1 = \rho \sin\theta \sin\phi \tag{I.5}$$

Substitution into eq I.2 gives

$$f^{(2)}(\mathbf{r}_1,\mathbf{r}_2) = f^{(2)}(x_1;x_1+\rho\cos\theta,\rho\sin\theta\cos\phi,\rho\sin\theta\sin\phi) \tag{I.6}$$

The function $f^{(2)}(\mathbf{r}_1,\mathbf{r}_2)$ must also remain invariant when the packing, locally assimilated to a slab, revolves as a

solid around the x_1 axis by an arbitrary angle ϕ_0

$$f^{(2)}(\mathbf{r}_1,\mathbf{r}_2) = f^{(2)}[x_1;x_1+\rho\cos\theta,\rho\sin\theta\cos(\phi-\phi_0),\rho\sin\theta\sin(\phi-\phi_0)] \quad \text{(I.7)}$$

Given the assumed symmetries, we can choose $\phi = \phi_0$, thus simplifying eq I.7 into eq 8 of the main text.

Appendix II

The contribution $g_1(\rho;\eta)$ to the function $g(\rho;\eta)$ is

$$g_1(\rho;\eta) = \frac{2}{\rho(1-\eta)^2}\left\{A_0\exp\left[t_0\left(\frac{\rho}{2}-1\right)\right] + \frac{2}{3}\exp\left[t_R\left(\frac{\rho}{2}-1\right)\right]\left\{\left[H_0-\frac{1}{2}(H_1+H_2)\right]\cos t_I\left(\frac{\rho}{2}-1\right)\right\} - \left(\frac{3}{4}\right)^{1/2}(H_1+H_2)\sin t_I\left(\frac{\rho}{2}-1\right)\right\} \quad \text{(II.1)}$$

where

$$A_0 = (H_0+H_1+H_2)/3 \quad \text{(II.2)}$$

$$H_0 = 1+\frac{1}{2}\eta \quad \text{(II.3)}$$

$$H_1 = \frac{-1}{4\eta\left(f^2+\frac{1}{8}\right)^{1/2}}[x_-^2(1-3\eta-4\eta^2)+x_+(1-2.5\eta^2)] \quad \text{(II.4)}$$

$$H_2 = \frac{1}{4\eta\left(f^2+\frac{1}{8}\right)^{1/2}}[x_+^2(1-3\eta-4\eta^2)+x_-(1-2.5\eta^2)] \quad \text{(II.5)}$$

$$t_0 = 2\eta\left(\frac{x_++x_--1}{1-\eta}\right) \quad \text{(II.6)}$$

$$t_I = 3^{1/2}\eta\left(\frac{x_+-x_-}{1-\eta}\right) \quad \text{(II.7)}$$

$$t_R = -\eta\left[\frac{2+(x_++x_-)}{1-\eta}\right] \quad \text{(II.8)}$$

$$f = \frac{(3+3\eta-\eta^2)}{4\eta^2} \quad \text{(II.9)}$$

$$x_+ = \left[f+\left(f^2+\frac{1}{8}\right)^{1/2}\right]^{1/3} \quad \text{(II.10)}$$

$$x_- = \left[f-\left(f^2+\frac{1}{8}\right)^{1/2}\right]^{1/3} \quad \text{(II.11)}$$

Supporting Information Available: Additional experimental information for this paper, including Figures 1S−9S. This material is available free of charge via the Internet at http://pubs.acs.org.

Nomenclature

a = frequency factor
A_T = cross-sectional area of the working walls, m^{-2}
b = damping coefficient
C = constant defined in eq 2, m^{-3}
$f^{(1)}(\mathbf{r}_1)$ = probability distribution of one bead with its center at position $\mathbf{r}_1$, m^{-3}
$f^{(2)}(\mathbf{r}_1,\mathbf{r}_2)$ = probability distribution of a pair of beads, m^{-6}
$g(\mathbf{r}_1,\mathbf{r}_2)$ = correlation function defined in eq 5
$H(x)$ = heaviside step function
n_∞ = bead centers per unit packing volume in the core region, m^{-3}
$N(x)$ = cumulative number of beads, m^{-3}
D_e = external diameter of the annular bed, m
D_i = internal diameter of the annular bed, m
r_p = average bead radius (=d_p/2), m
i = position vector with components (x_i, y_i, z_i) in a rectangular frame of reference
v_p = average bead volume, m^3
x = rectangular coordinate running along an axis perpendicular to the slab walls and increasing from either inward, measured as a multiple of the average bead radius
x_M = position of the midpoint between the two confining walls
x_0 = distance from where the second layer starts
y = generic position of the center of a bead

Greek Symbols

$\delta(x)$ = Dirac delta "function"
$\eta(x)$ = local volume fraction of solids at the position x
η_∞ = volume fraction of solids in the uniform core region
η_{cp} = mass volume fraction of a close-packed homogeneous arrangement
η_{LS} = mass volume fraction at the liquid-to-solid transition
$\varphi(x)$ = oscillating function defined in eq 3
z = variable of integration
(ρ, θ, ϕ) = spherical coordinate system centered at (x_1, y_1, z_1), with its $\theta = 0$ axis collinear to the x axis of the rectangular system
ρ = distance from the center of bead 1 to the center of bead 2 measured as a multiple of the average bead radius
ρ_{nc} = radius of the sphere enclosing the nearest couch of beads surrounding a central particle

Subscripts

exp = experimental value
th = theoretical value

Literature Cited

(1) Ollis, D. F., Al-Ekabi, H., Eds. *Photocatalytic Purification and Treatment of Water and Air*; Elsevier: New York, 1993.

(2) Hoffmann, M.; Martin, S.; Choi, W.; Bahnemann, D. Environmental Applications of Semiconductor Photocatalysis. *Chem. Rev.* **1995**, *95*, 69.

(3) Cassano, A. E.; Alfano, O. M. Reaction Engineering of Suspended Solid Heterogeneous Photocatalytic Reactors. *Catal. Today* **2000**, *58*, 167.

(4) Pozzo, R. L.; Giombi, J. L.; Baltanás, M. A.; Cassano, A. E. The Performance in a Fluidized Bed Reactor of Photocatalysts Inmobilized onto Inert Supports. *Catal. Today* **2000**, *62*, 175.

(5) Chiovetta, M. G.; Romero, R. L.; Cassano, A. E. Modeling of a Fluidized-Bed Photocatalytic Reactor for Water Pollution Abatement. *Chem. Eng. Sci.* **2001**, *56* (4), 1631.

(6) Crittenden, J. C.; Zhang, Y.; Hand, D. W.; Perram, D. L. Destruction of Organic Compounds in Water using Fixed-Bed Photocatalysts. *Solar Eng.* **1995**, *1*, 449.

(7) Raupp, G. B.; Nico, J. A.; Annangi, S.; Changrani, R.; Annapragada, R. Two-Flux Radiation-Field Model for an Annular Packed-Bed Photocatalytic Oxidation Reactor. *AIChE J.* **1997**, *43* (3), 792.

(8) Changrani, R.; Raupp, G. B. Performance Evaluation of a Titania-coated Reticulated Foam Photocatalytic Oxidation Reactor. *J. Adv. Oxid. Technol.* **1998**, *3* (3), 277.

(9) Changrani, R.; Raupp, G. B. Monte Carlo Simulation of the Radiation Field in a Reticulated Foam Photocatalytic Reactor. *AIChE J.* **1999**, *45* (5), 1085.

(10) Hossain, M. M.; Raupp, G. B. Polychromatic Radiation Field Model for a Honeycomb Monolith Photocatalytic Reactor. *Chem. Eng. Sci.* **1999**, *54*, 3027.

(11) Hossain, M. M.; Raupp, G. B.; Hay, S. O.; Obee, T. N. Three-Dimensional Developing Flow Model for Photocatalytic Monolith Reactors. *AIChE J.* **1999**, *45* (6), 1309.

(12) Zhang, Z.; Anderson, W. A.; Moo-Young, M. Rigorous Modeling of UV Absortion by TiO_2 Films in a Photocatalytic Reactor. *AIChE J.* **2000**, *46* (7), 1461.

(13) Esterkin, C. R.; Negro, A. C.; Alfano, O. M.; Cassano, A. E. Radiation Field Inside a Reactor of Glass-fiber Meshes Coated with TiO_2. *AIChE J.* **2002**, *48* (4), 832.

(14) Maruyama, T.; Nishimoto, T. Light Intensity Profile in Heterogeneous Photochemical Reactor. *Chem. Eng. Commun.* **1992**, *117*, 111.

(15) Ozisik, M. N. *Radiative Transfer and Interactions with Conduction and Convection*; John Wiley & Sons: New York, 1973.

(16) Siegel, R.; Howell, J. R. *Thermal Radiation Heat Transfer*, 3rd ed.; Hemisphere: Washington, DC, 1992.

(17) Mueller, G. Radial Void Fraction Correlation for Annular Packed Beds. *AIChE J.* **1999**, *45* (11), 2458.

(18) Martin, H. Low Peclet Number Particle-Fluid Heat and Mass Transfer in Packed Beds. *Chem. Eng. Sci.* **1978**, *33*, 913.

(19) Balescu, R. *Equilibrium and Nonequilibrium Statistical Mechanics*; John Wiley & Sons: New York, 1975; Chapter 3.

(20) Scott, G. D.; Charlesworth, A. M.; Mak, M. K. On the Random Packing of Spheres. *J. Chem. Phys.* **1964**, 611.

(21) Wertheim, M. S. Exact Solution of the Percus−Yevick Integral Equation for Hard Spheres. *Phys. Rev. Lett.* **1963**, *10* (8), 321.

(22) Scott, G. D. Packing of Spheres. *Nature* **1960**, *188* (4754), 908.

(23) Haughey, D. P.; Beveridge, G. S. G. Local Voidage Variation in a Randomly Packed Bed of Equal-sized Spheres. *Chem. Eng. Sci.* **1966**, *21*, 905.

Received for review December 9, 2002
Revised manuscript received December 16, 2003
Accepted December 17, 2003

IE020984W